

Role of Data Augmentation in Unsupervised Anomaly Detection

Jaemin Yoo¹, Tiancheng Zhao², Leman Akoglu¹

¹ Heinz College of Information Systems, Carnegie Mellon University

² School of Architecture, Carnegie Mellon University

jaeminyoo@cmu.edu, tianchen@andrew.cmu.edu, lakoglu@andrew.cmu.edu

Abstract

Self-supervised learning (SSL) has emerged as a promising alternative to create supervisory signals to real-world tasks, avoiding extensive cost of careful labeling. SSL is particularly attractive for unsupervised problems such as anomaly detection (AD), where labeled anomalies are costly to secure, difficult to simulate, or even nonexistent. A large catalog of augmentation functions have been used for SSL-based AD (SSAD), and recent works have observed that the type of augmentation has a significant impact on performance. Motivated by those, this work sets out to put SSAD under a larger lens and carefully investigate the role of data augmentation in AD through extensive experiments on many testbeds. Our main finding is that self-supervision acts as a yet-another model hyperparameter, and should be chosen carefully in regards to the nature of true anomalies in the data. That is, the alignment between the augmentation and the underlying anomaly-generating mechanism is the key for the success of SSAD, and in the lack thereof, SSL can even impair (!) detection performance. Moving beyond proposing another SSAD method, our study contributes to the better understanding of this growing area and lays out new directions for future research.

1 Introduction

Machine learning as a field has made tremendous progress in creating models that can learn from carefully labeled data. However, the cost of high-quality labeled data is a major bottleneck for the future of this supervised learning paradigm. Most recently, self-supervised learning (SSL) has emerged as a promising alternative to internally generate some kind of supervisory signal to solve a task. In essence, the unsupervised task is transformed into a supervised problem by auto-generating the labels. This new paradigm has had great success in advancing NLP (e.g., BERT (Devlin et al. 2019), XLM-R (Conneau et al. 2020), etc.) and has helped excel at various computer vision tasks (Goyal et al. 2021). Today, SSL is arguably the key toward “unlocking the dark matter of intelligence” (LeCun and Misra 2021).

SSL is particularly attractive for unsupervised learning problems such as anomaly detection (AD), as labeled data is (i) already rare/scarce or altogether nonexistent, (ii) costly to obtain by simulation (e.g. sandbox simulations in cybersecurity), or (iii) nontrivial to simulate in the face of unknown

Copyright © 2023, Association for the Advancement of Artificial Intelligence (www.aaai.org). All rights reserved.

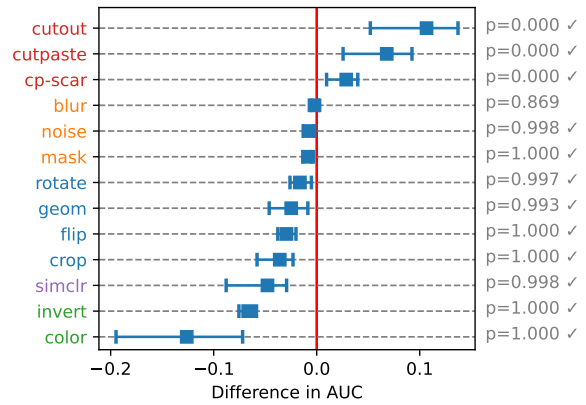


Figure 1: (best in color) Relative AUC w.r.t. the no-SSL baseline on the controlled testbed with anomaly-generating function gen:=CutOut. Color in augmentation names denotes their categories. Local augmentations (in red) work best due to the high alignment with gen, while others (e.g. in green) can even hurt (!) the accuracy significantly (p -values in gray). See our main findings (Obs. 1 and 2) in Sec. 4.1.

anomalies. As a result, the literature has seen a recent surge of SSL-based AD (SSAD) techniques (Golan and El-Yaniv 2018; Bergman and Hoshen 2020; Li et al. 2021; Qiu et al. 2021; Cheng et al. 2021; Shenkar and Wolf 2022). While these employ various different formulations (e.g., augmentation prediction, contrastive learning, etc.; see Sec. 2), as a common thread, they aim to learn how to distinguish normal data (or inliers) from self/auto-generated anomalies, the latter being input data (typically inlier-only) transformed via a what-is-called augmentation function.

Interestingly, a large catalog of different augmentation functions have been used in the SSAD literature – including rotation, flipping, cut-and-paste, blurring, masking, color jittering, etc. as well as “cocktail” augmentations as in GEOM (Golan and El-Yaniv 2018) and SimCLR (Chen et al. 2020) (See Sec. 3) – without any clear guidance on which one(s) to use on a new AD task. Alarmingly, there exist evidences in the literature that the choice of augmentation has significant impact on the outcome. As a motivating example, Li et al. (2021) have shown that on industrial defect detection (e.g. scratch on wood), a local augmentation such as CutPaste

works significantly better than a global one such as random rotation (90.9 vs. 73.1 AUC on avg., see their Table 1). In contrast, on semantic AD tasks where inliers and outliers are different object images from CIFAR-10 (Krizhevsky, Hinton et al. 2009), the *reverse* holds true (69.4 vs. 91.3 AUC, see their Sec. 5.4). They conclude that different type of AD tasks needs different augmentation designs.

Motivated by the above, this paper sets out to put SSAD under a larger lens and investigate the following questions:

1. **Success and failure (Sec. 4):** Does augmentation improve the vanilla model in all cases? Which augmentation functions perform best on certain types of anomalies?
2. **How augmentation works (Sec. 5):** How does augmentation function? What changes does it incur on error distributions and data representations of a detector f ?

Through extensive experiments on controlled testbeds as well as in-the-wild datasets, we find that self-supervision is **not** a “magic stick” for unsupervised AD, and rather remains to be a (yet-another) model hyperparameter—the choice of which heavily influences performance. Specifically, we observe that the alignment between the augmentation function aug and anomaly-generating function gen is essential to the success of SSAD, and it can even impair performance if the alignment is poor (depicted in Fig. 1). The alignment is determined not only by the type of aug , but also by its continuous parameters that affect the amount of augmentation.

Our observations are supported by various previous works on SSAD (details in Sec. 6). For example, Golan and El-Yaniv (2018) showed that geometric transformations such as rotation or flipping are suitable for detecting semantic class anomalies in image data, while Li et al. (2021) designed new augmentation functions to detect local defects in images of various objects. These works present partial evidence to our observed phenomena, while our work is the first formal comprehensive study to provide comprehensive evidence.

Our work aims to better understand existing approaches in a growing research field instead of proposing a new one. Being a systematic measurement study, this work is similar to those in other domains (Erhan et al. 2010; Mesquita, Jr., and Kaski 2020; Ruff et al. 2020) that also aim to critically review or understand growing areas. Three notable advantages of such studies include: they (i) put novel approaches in a growing area under a critical lens, (ii) shed light onto their working assumptions via carefully designed experiments, and (iii) pinpoint potential loopholes and misleading beliefs. We expect that our analyses will provide a better understanding of the role of SSL for AD and help steer the future directions of research on the topic.

2 Notations and Related Works

We first introduce notation and present recent approaches on self-supervised learning for anomaly detection (SSAD).

2.1 Notations

We define the problem of anomaly detection as follows. Let $\text{gen}(\cdot) : \mathbb{R}^d \rightarrow \mathbb{R}^d$ be an anomaly-generating function, and $p(\mathbf{x})$ and $p_{\text{gen}}(\mathbf{x})$ be the distributions of normal (or inlier) and anomalous (or outlier) data, respectively, where $\mathbf{x} \in \mathbb{R}^d$.

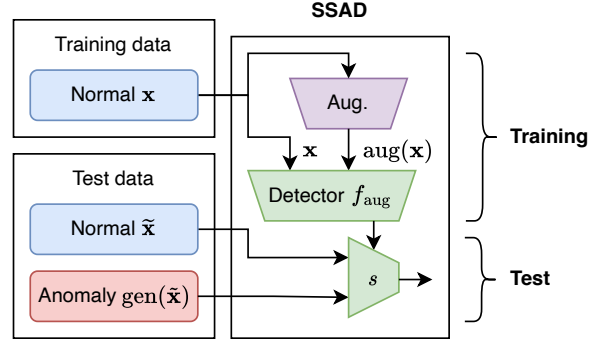


Figure 2: An overview of self-supervised anomaly detection (SSAD). Our goal is to study the role of the augmentation function aug with respect to the unknown anomaly-generating function gen that exists only in test data.

Given a set $\{\mathbf{x} \mid \mathbf{x} \sim p(\mathbf{x})\}$ of normal training data, the goal is to learn a score function $s : \mathbb{R}^d \rightarrow \mathbb{R}^1$ such that $s(\mathbf{x}') > s(\mathbf{x})$ if \mathbf{x}' is anomalous and \mathbf{x} is normal. We denote by D_{gen} a dataset whose anomalies are generated by gen .

We also define self-supervised anomaly detection (SSAD) as a training scheme of s that involves a set \mathcal{U} of augmentation functions. Each augmentation function $\text{aug} : \mathbb{R}^d \rightarrow \mathbb{R}^d$ modifies an example \mathbf{x} while preserving its semantic information, such as by adding Gaussian noise to each element of \mathbf{x} . In most cases, the target of training is typically a neural network f , and the score function s is defined on top of the data representations learned by f . We denote a network trained with aug by f_{aug} . Fig. 2 illustrates the overall process of SSAD to train a detector network f_{aug} .

The main focus of our study is the alignment $d(\text{aug}, \text{gen})$ between functions aug and gen . However, it is not straightforward to formally define $d(\cdot, \cdot)$ in image data, where pixel-level distances are not matched with semantic or visual differences. Thus, we say that aug and gen are *aligned* if they create visually similar outputs or work in a similar fashion, as given by our categorization of augmentation functions in Sec. 3, and they are perfectly aligned if $\text{aug} = \text{gen}$.

2.2 Generative Models

Generative models learn the distribution of normal data and predict an unseen example as an anomaly if it does not follow the learned distribution. Traditional autoencoder models (Zhou and Paffenroth 2017; Chen and Konukoglu 2018; Zong et al. 2018), generative adversarial networks (Schlegl et al. 2017; Zenati et al. 2018a,b; Akcay, Abarghouei, and Breckon 2018), and flow-based models (Yu et al. 2021; Gudovskiy, Ishizaka, and Kozuka 2022; Rudolph et al. 2022) are popular categories of generative models.

Recent works (Cheng et al. 2021; Ye et al. 2022) propose generative models for SSAD in the framework of denoising autoencoders (DAE), which involve an augmentation function aug to add noise to each input sample. Although traditional works (Vincent et al. 2008, 2010) used elementwise Gaussian noise or Bernoulli masking as aug , recent works have shown that more complex domain-specific augmentation such as random rotation in images is helpful to learn the

semantic information of data, achieving higher accuracy on anomaly detection (Cheng et al. 2021; Ye et al. 2022).

2.3 Augmentation Prediction

One popular approach for SSAD is to create samples with pseudo labels via multiple augmentation functions to learn a classifier. Given $\mathcal{U} = \{\text{identity}, \text{aug}_1, \dots, \text{aug}_N\}$, where $\text{identity}(\mathbf{x}) = \mathbf{x}$, the task is to conduct $(N+1)$ -way classification for predicting the function $\text{aug} \in \mathcal{U}$ given $\text{aug}(\mathbf{x})$. In this way, a classifier f is trained to differentiate different augmentation functions and then used to generate better representations of \mathbf{x} in one of its intermediate layers.

Many augmentation functions were proposed for anomaly detection in this sense, including geometric transformation (Golan and El-Yaniv 2018), patch rearranging (Wang et al. 2019), random affine transformation (Bergman and Hoshen 2020), local image transformation (Li et al. 2021), and learnable neural network-based transformation (Qiu et al. 2021). Some of them adopt existing augmentation functions to the task of anomaly detection, while some propose new ones.

2.4 Contrastive Learning

Contrastive learning is similar to augmentation prediction in that multiple augmentation functions are used to compose an objective function. The main difference is that contrastive learning utilizes pairs of augmentation functions and learns an estimator to produce similar outputs for the positive pairs, while augmentation prediction considers each function aug as an independent label to predict as classification.

Many previous works (Tack et al. 2020; Sehwag, Chiang, and Mittal 2021) based on contrastive learning use SimCLR (Chen et al. 2020) to create a set of positive samples. That is, the objective function is to learn similar representations for raw data and those transformed by SimCLR. The difference between various works is how they compose the set of negative samples, whose representations are learned to be farther from those of the positive ones. There is also a recent work that proposes a new augmentation function for contrastive learning on tabular data (Shenkar and Wolf 2022).

3 Experimental Setup

Model Among various models for anomaly detection, we adopt a denoising autoencoder (DAE) (Vincent et al. 2008, 2010) as the target model of experiments due to the following reasons. First, DAEs have been used widely in anomaly detection due to their robustness and generalizability (Cheng et al. 2021; Ye et al. 2022). Second, the training of DAEs is done simply by minimizing the reconstruction error without requiring additional regularizer terms. Third, DAEs support the *vanilla* version that works *without* augmentation, which is considered as the no-SSL base model for comparison. Finally, as DAEs learn to reconstruct the original sample from its corrupted (in our case, augmented) version, in effect they produce the counterfactual of an anomaly at the output, helping with the interpretation of anomalies at test/decision time. Detailed information on the model is in Appendix A.

Training and Inference The training of a DAE f is done by minimizing the following objective function:

$$l(\theta) = \mathbb{E}_{\mathbf{x}' \sim p_{\text{aug}}(\mathbf{x})} [\|f(\mathbf{x}'; \theta) - \mathbf{x}\|_2^2 + \lambda \|\theta\|_2^2], \quad (1)$$

where θ is the set of all learnable parameters of f , aug is an augmentation function (or a noise function in the context of traditional works), $p_{\text{aug}}(\mathbf{x})$ is a distribution of samples made by aug , and λ is a strength regularization. The training of a *vanilla* (i.e. no-SSL) AE is done by employing the identity augmentation function $\text{aug}(\mathbf{x}) = \mathbf{x}$ to Eq. (1).

After training a DAE, we use the mean squared error $r(\mathbf{x})$ between an input \mathbf{x} and the reconstructed one $\hat{\mathbf{x}}$ to compute an anomaly score. Specifically, given a test set \mathcal{T} containing both normal data and anomalies, we define the score $s(\mathbf{x})$ of \mathbf{x} as the percentile of $r(\mathbf{x})$ in \mathcal{T} . That is, \mathbf{x} is predicted as an anomaly if $r(\mathbf{x})$ is relatively high. We evaluate the DAE by measuring the area under the ROC curve (AUC) of scores.

Datasets Our experiments are conducted on two kinds of testbeds. The first is *in-the-wild* testbed, which is to select a single semantic class as normal and another class as anomalous. We include four different image datasets in this testbed: MNIST (LeCun et al. 1998), FashionMNIST (Xiao, Rasul, and Vollgraf 2017), SVHN (Netzer et al. 2011), and CIFAR-10 (Krizhevsky, Hinton et al. 2009). Since all datasets have 10 different classes, we have 90 pairs of normal and anomalous classes for each dataset. The second is *controlled* testbed, where we adopt a known augmentation function as the anomaly-generating function gen to have the full control of anomalies. Given SVHN and CIFAR-10, we apply three aug functions with limited randomness and different characteristics from each other: CutOut, Flip, and Invert. We denote these datasets by SVHN-C and CIFAR-10C, respectively.

Augmentation Functions We study various types of augmentation functions, which are categorized into five groups. The bullet colors are the same as in Figs. 1 and 4.

- **Geometric:** Crop (Chen et al. 2020), Rotate, Flip, and GEOM (Golan and El-Yaniv 2018).
- **Local:** CutOut (Devries and Taylor 2017; Zhong et al. 2017), CutPaste and CutPaste-scar (Li et al. 2021).
- **Elementwise:** Blur (Chen et al. 2020), Noise, and Mask (Vincent et al. 2010).
- **Color-based:** Invert and Jitter (Chen et al. 2020).
- **Mixed:** SimCLR (Chen et al. 2020).

Geometric augmentations make global geometric changes to images such as by rotation or flipping. Local augmentations, in contrast, modify only a part of an image such as by erasing a small patch. Elementwise augmentations modify every pixel locally or individually. Color-based augmentations change color information, while mixed augmentations combine multiple categories of augmentation functions. Detailed information is given in Appendix B. Detailed information is given in Appendix ??.

4 Success and Failure of Augmentation

First, we investigate *when* augmentation succeeds or otherwise fails, by comparing various DAEs (with augmentation) with the *vanilla* (no-SSL) AEs on our testbeds.

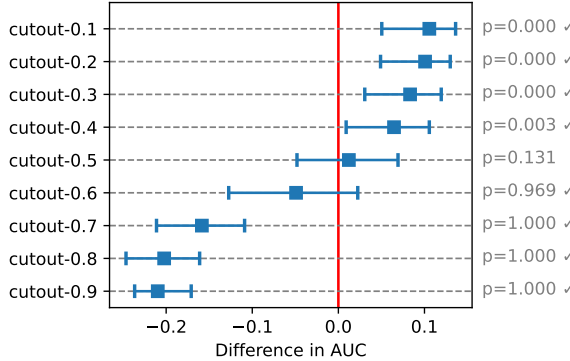


Figure 3: Relative AUC on the controlled testbed where the value of $c \in [0.1, 0.9]$ in $\text{aug} := \text{CutOut-}c$ depicts the size of erased patches. The anomaly function $\text{gen} := \text{CutOut}$ has an average size of patches ≈ 0.2 . Detection works better when c in aug is better aligned with that of gen . See Obs. 3.

Wilcoxon Tests We conduct each experiment for all possible pairs of classes and then run the paired Wilcoxon signed-rank test (Groggel 2000) between a DAE and the vanilla AE. For example, Fig. 1 shows the (pseudo)medians, 95% confidence intervals, and p -values as a result. The x -axis depicts the relative AUC compared with that of the vanilla AE. We consider that aug is beneficial (or disadvantageous) if the p -value is smaller than 0.05 (or larger than 0.95). We present only the main results, leaving details to Appendix C.

4.1 Controlled Testbed

First, we run experiments on the controlled testbed in which anomalies are generated by known augmentation functions. Figs. 1 and 3 show the results on $\text{gen} := \text{CutOut}$. Each row summarizes the AUC values on 20 tasks across two datasets (CIFAR-10C and SVHN-C) and ten classes each. We have the following observations from the results.

Observation 1 Given D_{gen} , DAE f_{aug} outperforms $f_{\text{aug}'}$ if aug is better aligned with gen than aug' is.

Observation 2 DAE f_{aug} impairs the accuracy of vanilla f if the alignment between aug and gen is poor in D_{gen} .

We show in Fig. 1 the relative AUC of DAE f_{aug} with various choices of aug . The local augmentation functions that exhibit the best alignment with $\text{gen} := \text{CutOut}$ significantly improve the vanilla AE. On the other hand, the remaining functions make negligible changes or even cause significant decrease in AUC. This demonstrates the importance of the alignment between aug and gen , and shows that DAEs can perform worse than the baseline under poor alignment. Our observations are consistent with other choices of gen , specifically Flip and Invert, as shown in Appendix C.1.

It is notable that the augmentations of the same category (i.e. the same color) are located together in the figure, implying that similar augmentation functions have similar characteristics even though their specifics are different. For example, CutOut works best because it is the perfect match with gen , while CutPaste and CutPaste-scar still perform well since they also augment a small image patch.

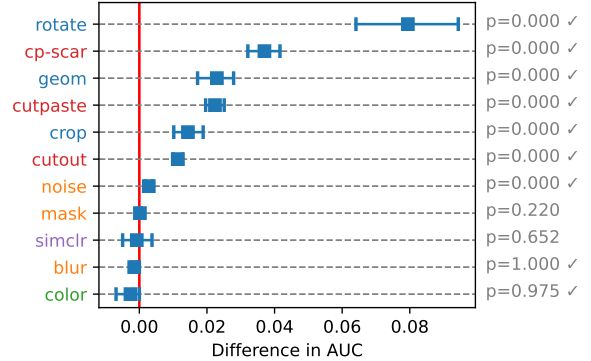


Figure 4: (best in color) Relative AUC on the in-the-wild datasets. Color in augmentation names represents their categories. The (blue) geometric and (red) local augmentations improve the no-SSL baseline. See Obs. 4 and 5.

Observation 3 The alignment between aug and gen in DAE f_{aug} is determined not only by the type of the function aug , but also by the amount of augmentation made by aug .

Fig. 3 compares multiple variants of CutOut- c , changing the width c of erased patches in augmented images. For example, CutOut-0.2 means that the width of erased patches is 20% of that of each image, making their area to 4%. Note that the original CutOut used as gen selects the patch width randomly in $(0.02, 0.33)$, making an average of 0.19.

The figure shows that CutOut- c is better with smaller c , and it starts to decrease the base AUC when $c \geq 0.6$. This is because CutOut- c with small c achieves the best alignment with gen , which also removes small patches of average size ≈ 0.2 . Even though the type of aug is the same as gen , the value of c determines whether f_{aug} succeeds or not.

4.2 In-the-Wild Testbed

Fig. 4 summarizes the results on 360 tasks across 4 datasets and 90 class pairs each, whose anomalies represent different semantic classes. Unlike in the controlled testbed, here the alignment between aug and gen is not known a priori. We have the following observations from the results, which are consistent also in individual datasets (see Appendix C.2).

Observation 4 Geometric aug performs best for datasets in which anomalies consist of different semantic classes.

Observation 5 SimCLR does not provide a meaningful improvement over the vanilla AE, although it is one of the most popular augmentation functions in the literature.

We observe from Fig. 4 that Rotate and other geometric augmentations perform well in semantic anomaly detection tasks. This implies that simple rotation achieves the best alignment between aug and gen , replicating the observation of a previous work (Li et al. 2021) introduced in Sec. 1. A plausible explanation is that many classes in those datasets, such as dogs and cats in CIFAR-10, are rotation-sensitive. Thus, the rotation by aug creates plausible samples outside the normal data distribution, giving f_{aug} an ability to differentiate anomalies that may look like rotated normal images. We support this claim by detailed analysis in Sec. 5.

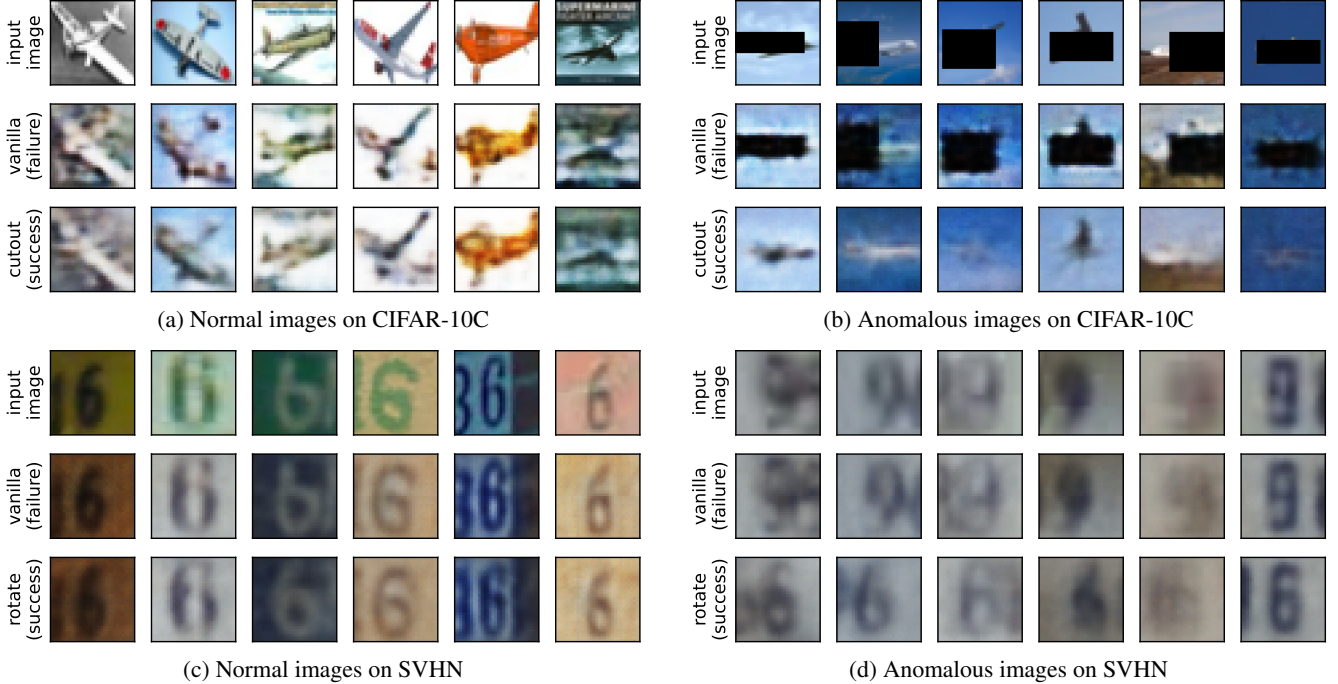


Figure 5: Images from CIFAR-10C and SVHN, where the three rows represent original images and those reconstructed by the vanilla AE and DAE, respectively. (a, b) $\text{aug} := \text{CutOut}$ and $\text{gen} := \text{CutOut}$. (c, d) $\text{aug} := \text{Rotate}$, and the digits of 6 and 9 are normal and anomalous classes, respectively. The **success** and **failure** represent whether the images are assigned accurately to their true classes (normal vs. anomaly). DAEs preserve the original images (on the left), while applying the inverse augmentation aug^{-1} to anomalies (on the right), making them resemble normal ones with high reconstruction errors. See Obs. 6 and 7.

Local augmentations also work well, since changes in image patches make objects presented in different ways, affecting the semantic class information. Nevertheless, the amount of improvement is not as large as in geometric ones.

A notable observation is that SimCLR, which is one of the most popular augmentation functions in the literature, does not introduce a significant improvement to the base model. This is because SimCLR is designed to *preserve* the semantic information of images while making pixel-level changes, while what DAEs require for aug is to *change* the semantic information for better alignment with gen .

5 How Augmentation Works

Next, we analyze how and why augmentation helps DAEs achieve better performance than the vanilla AE.

5.1 Case Studies

We visually inspect individual samples to observe what images DAEs reconstruct for normal versus anomalous inputs. Fig. 5 shows the results on CIFAR-10C and SVHN with different aug . We have the following observations.

Observation 6 *Given an anomaly $\text{gen}(\mathbf{x})$, a DAE f_{aug} approximates the inverse augmentation aug^{-1} if gen and aug are aligned well, satisfying $f(\text{gen}(\mathbf{x})) \approx \mathbf{x}$.*

Observation 7 *Given a normal sample $\mathbf{x} \sim p(\mathbf{x})$, a DAE f approximates the identity function, satisfying $f(\mathbf{x}) \approx \mathbf{x}$.*

In Fig. 5, we see that given normal images, both models reconstruct similar images giving low reconstruction errors,

but the vanilla AEs fail to predict them as normal since the errors are low also for the anomalous images. Given anomalies, the DAEs recover their counterfactual versions by applying the inverse augmentation function aug^{-1} , increasing their reconstruction errors to become higher than those from the normal images. This makes DAEs achieve higher AUC than vanilla AEs. We derive the same observations from different gen functions on both testbeds (see Appendix D).

It is notable that the task of detecting digits 9 as anomalous from digits 6 is *naturally aligned* with the Rotate augmentation, since in effect, the DAE learns the images of rotated 6 to be anomalies. This alignment is an essential factor for the success of SSAD as we claim in Obs. 1 and 2.

5.2 Error Histograms

Next we study the effect of augmentation functions on the reconstruction error distributions of the normal samples and anomalies. Fig. 6 shows the histograms of errors on CIFAR-10C. We make the following observations from the results, which are consistent with different gen functions in the controlled and in-the-wild testbeds (see Appendix E).

Observation 8 *The overall reconstruction errors are higher in DAEs than in the vanilla AEs.*

Observation 9 *The reconstruction errors increase in overall with the degree of change that augmentation employs.*

We compare DAEs with three different aug functions and the vanilla AE in Fig. 6. The DAEs show higher reconstruction errors in general than the vanilla AE, providing more

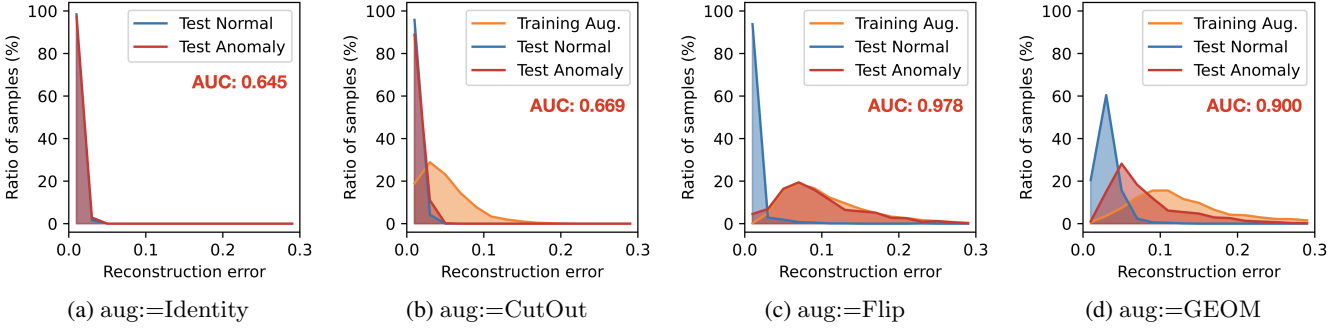


Figure 6: (best in color) Reconstruction error on CIFAR-10C with Automobile as the normal class and gen:=Flip. The distributions gradually shift to the right as the augmentation aug changes the input images more and more: (a) Identity, (b) CutOut (local), (c) Flip (global), and (d) GEOM (“cocktail” augmentation). The distributions of augmented samples and anomalies are matched the most in (c) when $\text{aug} = \text{gen}$, which means the perfect alignment. See Obs. 8 and 9.

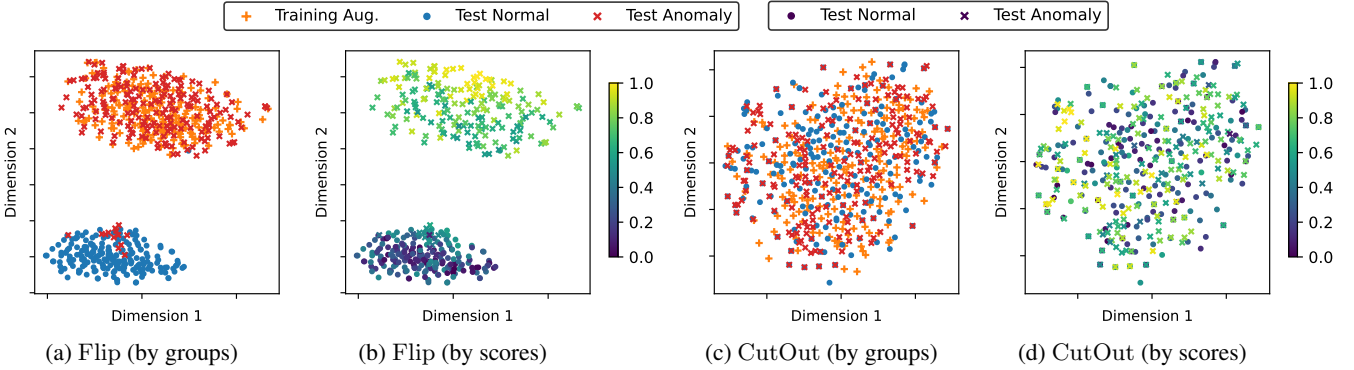


Figure 7: (best in color) t -SNE visualization of embeddings on CIFAR-10C when $\text{aug} = \text{gen}$: (a, b) $\text{aug} = \text{gen} = \text{Flip}$ and (c, d) $\text{aug} = \text{gen} = \text{CutOut}$. The colors represent either (a, c) data categories or (b, d) anomaly scores. It achieves high AUC of 0.978 and 0.973 in both cases, respectively, despite the distributions of their embeddings are different geometrically. See Obs. 10.

right-shifted error distributions. This is because the objective function of DAEs involves a denoising term that increases the reconstruction errors for augmented data. The improved AUC of DAEs is the result of increasing the reconstruction errors for anomalies than those for normal data.

In Fig. 6, the amount of change incurred by an augmentation aug increases from (6a) to (6d). The error distributions are shifted to the right accordingly, as augmented data become more distant from the normal data. Notably, the distribution for the true anomalies is more right-shifted in Fig. 6c than in Fig. 6d, showing the higher AUC of 0.978, thanks to the better alignment between aug and gen.

5.3 Embedding Visualization

Figs. 7 and 8 show embeddings on CIFAR-10C and CIFAR-10, respectively, learned by various augmentation functions. We have the following observations from the results.

Observation 10 *Embeddings from a DAE f_{aug} for normal and anomalous data are separated when aug makes global changes, whereas mixed when aug makes local changes.*

The first two and the last two plots in Fig. 7 exhibit different scenarios. In Figs. 7a and 7b, there are separate clusters: one for normal data, and another for augmented and anomalous data. In Figs. 7c and 7d, all data points compose a single

cluster without a clear separation between the different categories. The difference between the two scenarios is driven by the characteristic of aug: Flip makes global changes in images, while CutOut affects only a part of each image.

Observation 11 *Augmentation can work even under imperfect alignment if the anomalies lie between the normal and augmented data in the embedding space.*

Fig. 8 visualizes the result on CIFAR-10 with semantic anomalies and $\text{aug} = \text{Rotate}$. The alignment between aug and gen is not perfect, which is shown by the separation between the augmented data and the anomalies in the embedding space; the augmented points make four separate clusters based on the four degree options of Rotate, which are $\{0, 90, 180, 270\}$. Nevertheless, the augmentation improves the vanilla AE, since the anomalies lie between normal and augmented data in the embedding space.

We also study the cases of different gen functions in Appendix F, including both success and failure scenarios. The failure case of SimCLR creates an isolated cluster of augmented samples, which misguides the training of f .

6 Discussion

We present further discussion on our experiments and observations, in the context of prior related works.

Table 1: AUC of the GEOM model on CIFAR-10. The first four rows use the original GEOM augmentation, while the last four use CutPaste. The columns represent classes treated as normal at each experiment. **Semantic** means the semantic anomalies of different classes in the one-vs-rest scheme, while **CutOut**, **Invert**, and **Flip** mean anomalies constructed via augmentation as in the other experiments. GEOM model works better with a better alignment, consistent with our main Obs. 1 and 2.

Augment	Anomaly	Air.	Auto.	Bird	Cat	Deer	Dog	Frog	Horse	Ship	Truck	Average
GEOM	Semantic	0.737	0.958	0.782	0.731	0.875	0.875	0.854	0.956	0.940	0.914	0.862
GEOM	CutOut	0.841	0.910	0.866	0.704	0.797	0.797	0.831	0.820	0.812	0.745	0.812
GEOM	Invert	0.820	0.961	0.794	0.730	0.925	0.880	0.810	0.956	0.925	0.982	0.878
GEOM	Flip	0.724	0.998	0.948	0.873	0.988	0.968	0.959	0.999	0.988	0.995	0.944
CutPaste	Semantic	0.523	0.533	0.561	0.558	0.543	0.593	0.617	0.566	0.481	0.507	0.548
CutPaste	CutOut	0.979	0.999	1.000	0.999	1.000	0.998	1.000	1.000	0.991	1.000	0.997
CutPaste	Invert	0.436	0.625	0.629	0.619	0.718	0.540	0.803	0.638	0.493	0.605	0.610
CutPaste	Flip	0.500	0.491	0.475	0.489	0.487	0.473	0.471	0.482	0.512	0.493	0.488

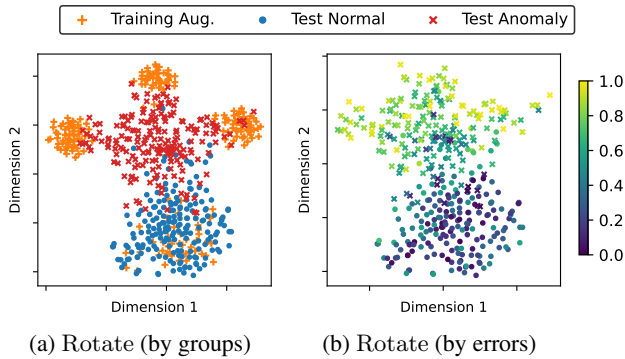


Figure 8: (best in color) t-SNE visualization of embeddings on CIFAR-10 with Automobile (normal) vs. Cat (anomaly). We set aug:=Rotate in both figures. Colors depict either (a) data categories or (b) anomaly scores. See Obs. 11.

6.1 Generalization to Other Models

This work studied denoising autoencoders (DAE) as the target model, yet our observations continue to hold with other SSAD models. To that end, we also conduct experiments on the GEOM model that uses augmentation prediction (Golan and El-Yaniv 2018) as the objective function (see Sec. 2.3). Table 1 presents the AUC of the GEOM model on CIFAR-10 with various types of anomalies: different object classes and anomalies constructed from known augmentation functions. With the original GEOM augmentation as aug, the model achieves the highest AUC when gen:=Flip. This is because Flip is a special case of the GEOM augmentation. With the CutPaste augmentation, on the other hand, the model works best when gen:=CutOut that aligns relatively well with aug, yet significantly poorly in other cases.

6.2 Insights from Previous Works

We introduce previous works for SSAD that present insights consistent with our observations about the importance of the alignment between aug and the nature of true anomalies.

Golan and El-Yaniv (2018) observed that geometric transformations perform better than non-geometric ones such as Gaussian blurring or image sharpening on detecting semantic anomalies. Hendrycks et al. (2019) found that rotation prediction helps detect harder anomalies located near the decision boundary between normal and anomalous data. Li

et al. (2021) showed that local augmentation functions that focus on small perturbations of images better capture defects and flaws appearing in anomalous objects, and work significantly superior to global augmentations such as rotation.

Ye, Chen, and Zheng (2021) identified that any supervisory signal given to the training of an anomaly detector induces a bias, which distorts the score distribution of the detector toward the given signals ignoring the relationships between classes. Since data augmentation in SSAD works as a generator of supervisory signals, the alignment between aug and gen determines the possible direction of bias.

Tack et al. (2020) and Sohn et al. (2021) noticed that *hard* augmentations such as random rotation can shift the sample distribution and harm the performance of contrastive learning for anomaly detection. Their observations imply that the optimal choice of augmentation depends not only on the nature of anomalies, but also the objective function used in the training as it introduces a different requirement for aug.

Qiu et al. (2021) proposed to learn an augmentation function aug as a neural network jointly with an anomaly detector f to automatically adapt to given datasets. Nevertheless, the training is done only for the differentiable parameters in aug, however the function *family* of parameterized augmentations (i.e., its network structure and hyperparameters) is left to be pre-specified manually.

7 Conclusion

In this work, we studied the role of self-supervised learning (SSL) in unsupervised anomaly detection (AD). Through carefully set-up experiments on numerous datasets and extensive analyses, we showed that the alignment between augmentation and the anomaly-generating mechanism plays an essential role in the success of SSL; and importantly, SSL may even hurt detection performance under poor alignment. As such, SSL for AD emerges as a data-specific solution, rather than a general cure-all panacea, effectively rendering it a model hyperparameter—nontrivial to specify in fully unsupervised settings. Our study is motivated (and findings are also supported) by various partial evidences reported in previous works, and serves as the first systematic large-scale study to provide comprehensive evidence. We expect our work will trigger future research on the better understanding of this growing area, in addition to principled SSL for AD techniques that can tackle the outlined challenges.

References

Akcay, S.; Abarghouei, A. A.; and Breckon, T. P. 2018. GANomaly: Semi-supervised Anomaly Detection via Adversarial Training. In *ACCV*.

Bergman, L.; and Hoshen, Y. 2020. Classification-Based Anomaly Detection for General Data. In *ICLR*.

Chen, T.; Kornblith, S.; Norouzi, M.; and Hinton, G. E. 2020. A Simple Framework for Contrastive Learning of Visual Representations. In *ICML*.

Chen, X.; and Konukoglu, E. 2018. Unsupervised Detection of Lesions in Brain MRI using constrained adversarial auto-encoders. *CoRR*, abs/1806.04972.

Cheng, Z.; Zhu, E.; Wang, S.; Zhang, P.; and Li, W. 2021. Unsupervised Outlier Detection via Transformation Invariant Autoencoder. *IEEE Access*, 9: 43991–44002.

Conneau, A.; Khandelwal, K.; Goyal, N.; Chaudhary, V.; Wenzek, G.; Guzmán, F.; Grave, E.; Ott, M.; Zettlemoyer, L.; and Stoyanov, V. 2020. Unsupervised Cross-lingual Representation Learning at Scale. In *ACL*.

Devlin, J.; Chang, M.; Lee, K.; and Toutanova, K. 2019. BERT: Pre-training of Deep Bidirectional Transformers for Language Understanding. In *NAACL-HLT*.

Devries, T.; and Taylor, G. W. 2017. Improved Regularization of Convolutional Neural Networks with Cutout. *CoRR*, abs/1708.04552.

Erhan, D.; Bengio, Y.; Courville, A. C.; Manzagol, P.; Vincent, P.; and Bengio, S. 2010. Why Does Unsupervised Pre-training Help Deep Learning? *J. Mach. Learn. Res.*, 11: 625–660.

Golan, I.; and El-Yaniv, R. 2018. Deep Anomaly Detection Using Geometric Transformations. In *NeurIPS*.

Goyal, P.; Caron, M.; Lefauveaux, B.; Xu, M.; Wang, P.; Pai, V.; Singh, M.; Liptchinsky, V.; Misra, I.; Joulin, A.; and Bojanowski, P. 2021. Self-supervised Pretraining of Visual Features in the Wild. *CoRR*, abs/2103.01988.

Groggel, D. J. 2000. Practical Nonparametric Statistics. *Technometrics*, 42(3): 317–318.

Gudovskiy, D. A.; Ishizaka, S.; and Kozuka, K. 2022. CFLOW-AD: Real-Time Unsupervised Anomaly Detection with Localization via Conditional Normalizing Flows. In *WACV*.

Hendrycks, D.; Mazeika, M.; Kadavath, S.; and Song, D. 2019. Using Self-Supervised Learning Can Improve Model Robustness and Uncertainty. In *NeurIPS*.

Krizhevsky, A.; Hinton, G.; et al. 2009. Learning multiple layers of features from tiny images.

LeCun, Y.; Bottou, L.; Bengio, Y.; and Haffner, P. 1998. Gradient-based learning applied to document recognition. *Proc. IEEE*, 86(11): 2278–2324.

LeCun, Y.; and Misra, I. 2021. Self-supervised learning: The dark matter of intelligence.

Li, C.; Sohn, K.; Yoon, J.; and Pfister, T. 2021. CutPaste: Self-Supervised Learning for Anomaly Detection and Localization. In *CVPR*.

Mesquita, D. P. P.; Jr., A. H. S.; and Kaski, S. 2020. Rethinking pooling in graph neural networks. In *NeurIPS*.

Netzer, Y.; Wang, T.; Coates, A.; Bissacco, A.; Wu, B.; and Ng, A. Y. 2011. Reading digits in natural images with unsupervised feature learning.

Qiu, C.; Pfrommer, T.; Kloft, M.; Mandt, S.; and Rudolph, M. 2021. Neural Transformation Learning for Deep Anomaly Detection Beyond Images. In *ICML*.

Rudolph, M.; Wehrbein, T.; Rosenhahn, B.; and Wandt, B. 2022. Fully Convolutional Cross-Scale-Flows for Image-based Defect Detection. In *WACV*.

Ruff, L.; Vandermeulen, R. A.; Franks, B. J.; Müller, K.; and Kloft, M. 2020. Rethinking Assumptions in Deep Anomaly Detection. *CoRR*, abs/2006.00339.

Schlegl, T.; Seeböck, P.; Waldstein, S. M.; Schmidt-Erfurth, U.; and Langs, G. 2017. Unsupervised Anomaly Detection with Generative Adversarial Networks to Guide Marker Discovery. In *IPMI*.

Sehwag, V.; Chiang, M.; and Mittal, P. 2021. SSD: A Unified Framework for Self-Supervised Outlier Detection. In *ICLR*.

Shenkar, T.; and Wolf, L. 2022. Anomaly Detection for Tabular Data with Internal Contrastive Learning. In *ICLR*.

Sohn, K.; Li, C.; Yoon, J.; Jin, M.; and Pfister, T. 2021. Learning and Evaluating Representations for Deep One-Class Classification. In *ICLR*.

Tack, J.; Mo, S.; Jeong, J.; and Shin, J. 2020. CSI: Novelty Detection via Contrastive Learning on Distributionally Shifted Instances. In *NeurIPS*.

Vincent, P.; Larochelle, H.; Bengio, Y.; and Manzagol, P. 2008. Extracting and composing robust features with denoising autoencoders. In *ICML*.

Vincent, P.; Larochelle, H.; Lajoie, I.; Bengio, Y.; and Manzagol, P. 2010. Stacked Denoising Autoencoders: Learning Useful Representations in a Deep Network with a Local Denoising Criterion. *J. Mach. Learn. Res.*, 11: 3371–3408.

Wang, S.; Zeng, Y.; Liu, X.; Zhu, E.; Yin, J.; Xu, C.; and Kloft, M. 2019. Effective End-to-end Unsupervised Outlier Detection via Inlier Priority of Discriminative Network. In *NeurIPS*.

Xiao, H.; Rasul, K.; and Vollgraf, R. 2017. Fashion-MNIST: a Novel Image Dataset for Benchmarking Machine Learning Algorithms. *CoRR*, abs/1708.07747.

Ye, F.; Huang, C.; Cao, J.; Li, M.; Zhang, Y.; and Lu, C. 2022. Attribute Restoration Framework for Anomaly Detection. *IEEE Trans. Multim.*, 24: 116–127.

Ye, Z.; Chen, Y.; and Zheng, H. 2021. Understanding the Effect of Bias in Deep Anomaly Detection. In *IJCAI*.

Yu, J.; Zheng, Y.; Wang, X.; Li, W.; Wu, Y.; Zhao, R.; and Wu, L. 2021. FastFlow: Unsupervised Anomaly Detection and Localization via 2D Normalizing Flows. *CoRR*, abs/2111.07677.

Zenati, H.; Foo, C. S.; Lecouat, B.; Manek, G.; and Chandrasekhar, V. R. 2018a. Efficient GAN-Based Anomaly Detection. *CoRR*, abs/1802.06222.

Zenati, H.; Romain, M.; Foo, C.; Lecouat, B.; and Chandrasekhar, V. 2018b. Adversarially Learned Anomaly Detection. In *ICDM*.

Zhong, Z.; Zheng, L.; Kang, G.; Li, S.; and Yang, Y. 2017. Random Erasing Data Augmentation. *CoRR*, abs/1708.04896.

Zhou, C.; and Paffenroth, R. C. 2017. Anomaly Detection with Robust Deep Autoencoders. In *KDD*.

Zong, B.; Song, Q.; Min, M. R.; Cheng, W.; Lumezanu, C.; Cho, D.; and Chen, H. 2018. Deep Autoencoding Gaussian Mixture Model for Unsupervised Anomaly Detection. In *ICLR*.